Sánchez-Prieto, J.; Hernández-Jiménez, F.; García-Gutiérrez, L.M.; Soria-Verdugo, A. (2017). Experimental study on the characteristic mixing time of solids and its link with the lateral dispersion coefficient in bubbling fluidized beds, *Chemical Engineering Journal*, v. 307, pp.: 113-121.

DOI: https://doi.org/10.1016/j.cej.2016.08.075

Experimental study on the characteristic mixing time of solids and its link with the lateral dispersion coefficient in bubbling fluidized beds

J. Sánchez-Prieto [a,*], F. Hernández-Jiménez[a], L.M. Garcia-Gutierrez[a], A. Soria-Verdugo[a]

[a] *Universidad Carlos III de Madrid, Thermal and Fluid Engineering Department, Avda. de la Universidad 30, 28911 Leganés (Madrid), Spain*

Abstract

An experimental relation between the characteristic mixing time of solids and the lateral dispersion coefficient in a bubbling fluidized bed is established in this work. To do that, experiments were carried out in a pseudo-2D fluidized bed using glass beads as bed material. The glass beads have the same density and diameter but half of them are painted in black to make them distinguishable. At the beginning of each experiment, the particles were placed in a completely lateral segregated state and then the fluidizing air was suddenly injected while images were recorded. The images were processed to obtain the mixing index evolution with time. Two different regions where differentiated in the evolution of the lateral mixing with time: a region dominated by convective mixing and a region governed by diffusive mixing. Both the start-up time and the total solids mixing time were characterized. The total solids mixing time was found to have a potential relation with the excess gas velocity and it was found to be independent of the particle size. This total solids mixing time was compared to the residence time of the bubbles in the bed and it was showed that the axial solids mixing is two orders of magnitude faster than the lateral solids mixing. This result justifies the use of the 1D Fickian-type diffusion equation to fit the experimental data of the mixing index obtaining the values of the lateral dispersion coefficient. Finally, the experimental values of the total solids mixing time were com-

*Corresponding author

Email address: jsprieto@ing.uc3m.es (J. Sánchez-Prieto)

pared to the experimental values of the lateral dispersion coefficient and a straightforward relation between both parameters was provided.

Keywords:
Solids mixing, Mixing index, Lateral dispersion coefficient, Pseudo-2D, Fluidized bed

---

1. Introduction

Bubbling gas-solid fluidized beds (BFBs) are broadly applied in industry, particularly in thermochemical energy conversion processes such as combustion and gasification. The fluidization process offers a high heat transfer rate, good solids mixing and handling, and provides a uniform and controllable temperature [1]. Moreover, its ability to process low grade fuels with low pollutant emission makes the use of BFBs a competitive technology for the valorization of biomass and wastes in mid-scale energy conversion processes.

A particular concern in the study of the fluidization process is the solids mixing rate, because such knowledge is very useful for the design of fuel feeding ports in fluidized bed boilers [2–4]. The mixing of particles influences the rates of heat and mass transfer in fluidized beds which is not fully understood because of its complexity [5]. In many cases, the proper mixing of particles is crucial to ensure uniform heating, reaction, or drying of the particles and also to prevent the formation of hot spots.

The basic mechanism of solids mixing in bubbling fluidized beds is known to be related to bubbles [6]. When a bubble rises through the bed, it carries a wake of particles to the bed surface and there is a permanent displacement or drift of the particles outside the bubble [7]. A downflow of solids exists in the region surrounding the rising bubbles, resulting on a convective circulation of particles in the axial direction of the bed. At the same time, lateral mixing of solids occurs caused partly by coalescence and partly by lateral dispersion of particles in the bubble wake at the bed surface due to the bubble eruption.

The study of the solids mixing in fluidized beds can be divided into two main groups. The first one corresponds to studies focused on the determination of the mixing time or mixing curves. One of the most used experimental techniques to obtain the mixing curves is marking part of the packed bed (e.g. using a particular colour). Then, the variation of concentration of the marked particles is monitored by means of external visualization. Since no extra particles are added to the bed and observation is made through

visualization from outside the bed, this method does not disturb the flow [6]. To allow the external visualization of the bed, most of these studies were conducted in pseudo-two-dimensional (pseudo-2D) beds, which has been fundamental for the understanding of the dynamics of gas-solid systems [8–17]. A few experimental studies related to the mixing curves can be found in the literature for both 2D and 3D facilities. Hull *et al.* [18] studied the mixing process of coloured particles with a video image analysis technique in a pseudo-2D fluidized bed with internals. Zhang *et al.* [19] reported experimental measurements on solids mixing in a spouted bed. Gorji-Kandi *et al.* [20] employed an experimental visualization technique to study several configurations of coloured particle layers in a pseudo-2D fluidized bed. Recently, Julián *et al.* [21, 22] studied the mixing process in a two-section two-zone fluidized bed reactor. Furthermore, there are many numerical investigations on this topic available in the literature, specially focused on DEM simulations [6, 23–26].

The second group corresponds to studies focused on the determination of the lateral dispersion coefficient. The objective of these works is to measure the overall dispersion of a batch of tracing particles and then fit the mixing curve with a 1D Fickian-type diffusion equation. In this way, the mixing induced by different factors is lumped as an effective dispersion coefficient. Bellgardt *et al.* [27] confirmed that vertical mixing was much faster than horizontal mixing, thus the use of one-dimensional dispersion model in the horizontal direction is justified. Regarding the estimation of the lateral dispersion coefficient, many experimental studies can be found in the literature. There are two different types of experimental works in this group: those based on the study of the mixing of bulk solids and those based on the study of individual objects immersed in the bed. Examples of the former type of works can be found in Borodulya *et al.* [28], Glicksman *et al.* [29] and Shen and Zhang [30], where experimental thermal tracing techniques to obtain the lateral dispersion coefficient were reported. Shi and Fan [31] obtained the lateral dispersion coefficient of bulk solids in a pseudo-2D fluidized bed with coloured particles. Sette *et al.* [32] also estimated the lateral dispersion coefficient using an indirect tracking method for bed material based on magnetic separation. Regarding the experimental works based on the study of mixing of individual particles, Bellgardt and Werther [33] employed a CO_2 sublimation technique in a fluidized bed pilot plant. Niklasson *et al.* [2] measured the gas concentration profile in a fluidized bed boiler. Mostoufi and Chaouki [34] studied the solids movement in a fluidized bed by means of Radioactive

Particle Tracking (RPT). Sette *et al.* [35] compared the experimental values of the lateral dispersion coefficient of several fuels. Recently, Sette *et al.* [36] studied the motion of individual fuel particles in the surface of a large-scale fluidized bed at high temperature by means of a camera-based fuel tracking system. A few numerical studies two-fluid models or DEM simulations can also be found in the literature [3, 37–39]. However, the values of dispersion coefficient in the literature are very scattered [2], which makes the results of previous studies on the dispersion coefficient difficult to generalize or to scale up.

In this work, the mixing process and the lateral dispersion coefficient in a pseudo-2D bubbling fluidized bed are linked experimentally. Pseudo-2D fluidized beds typically have a transparent front wall in order to allow optical access to the system and the back wall of the bed is separated to the front wall by a narrow distance to ensure that the visualization is representative of the whole process. These pseudo-2D beds are crucial for the understanding of the dynamics of gas-particle systems. The mixing curves and mixing time are obtained using a visualization technique. The experimental results of the mixing curves are also fitted to the Fick's Law in order to obtain values of the lateral dispersion coefficient. As a novelty, the experimental procedure begins from a completely lateral segregated state, which allows to link the characteristic mixing time of solids with the lateral dispersion coefficient. The effect of the gas superficial velocity and the particle size on both parameters is studied. The experimental values of the lateral dispersion coefficient are finally compared with the predictions of correlations that can be found in the literature.

2. Experimental setup

The experimental facility employed in this work is a pseudo-2D cold fluidized bed of dimensions 0.3 m x 1 m x 0.01 m (width W, height H, and thickness Z). A schematic diagram of the experimental setup is shown in Figure 1. The bed was filled with ballotini glass particles of 2500 kg/m^3 density. The experiments were carried out for three different particle sizes of 0.4-0.6 mm, 0.6-0.8 mm and 1-1.3 mm diameter. The tracer particles employed were the same ballotini glass particles previously painted in black. The black coating is thin enough to consider that the physical properties of the particles (shape, size and density) are the same as the non-painted

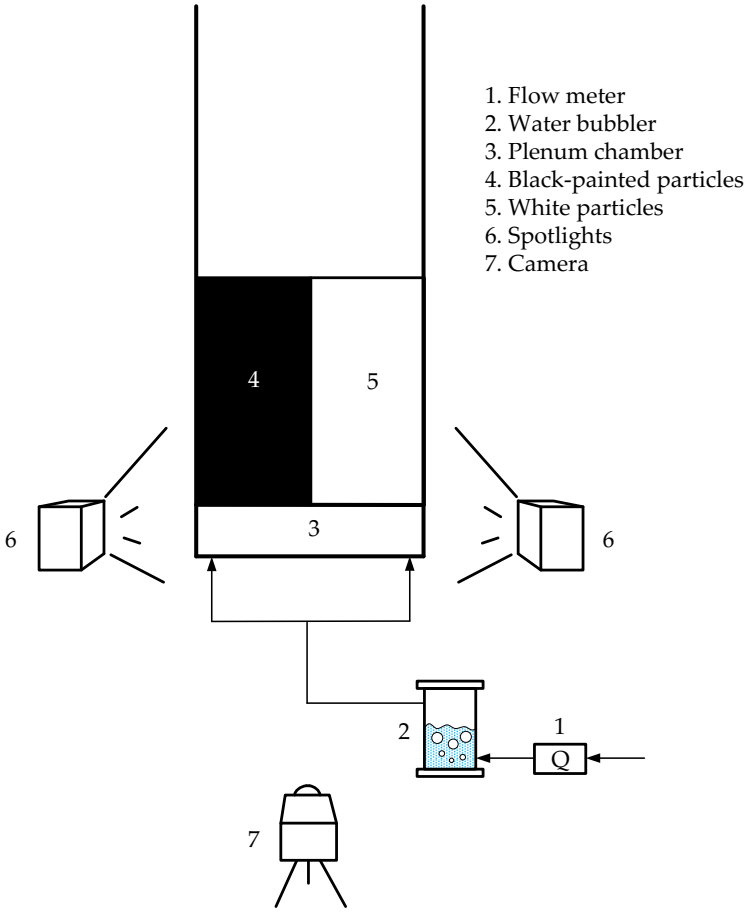

Figure 1: Schematic diagram of the experimental setup.

particles, as can be seen in the Scanning Electron Microscope (SEM) images of Figure 2.

The air flow was measured with a set of two flow meters, with ranges of $0 - 200$ L/min and $0 - 500$ L/min providing an accuracy of 1% of full-scale span (FSS), which means a measurement uncertainty of 2 and 5 l/min respectively. The gas distributor consists of a perforated plate with two rows

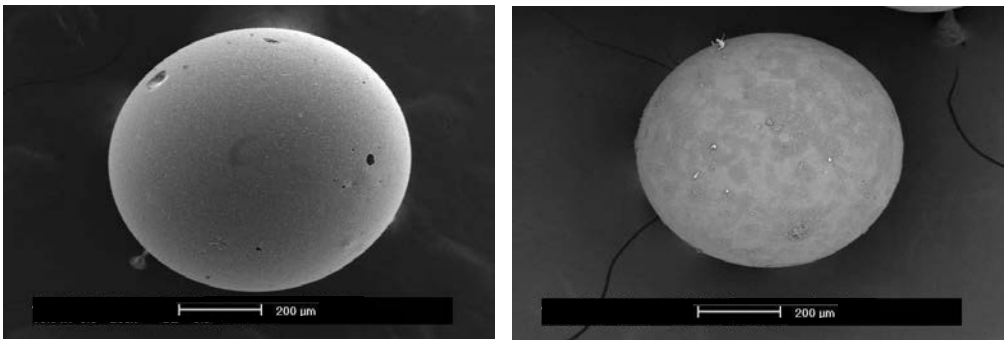

(a) (b)

Figure 2: SEM images of non-painted particles (a) and black painted particles (b).

of 30 holes of 1 mm diameter arranged in a triangular configuration with 1 cm pitch. The pressure drop of the distributor plate is $\Delta P_{dist} = 4.65 U_0^2$. The distributor is equipped with a mesh to avoid the falling of particles inside the plenum chamber and to ensure a proper distributor to bed pressure drop ratio, R, to avoid gas maldistribution [40, 41]. The front and rear walls of the bed were made of glass and the rear wall was painted in black to increase contrast in the front image. A summary of the experimental parameters is included in Table 1.

Table 1: Summary of experimental conditions.

Parameter		Value
Bed height, H(m)		1
Bed width, W(m)		0.3
Bed thickness, Z(m)		0.01
Aspect ratio, H_0/W (-)		1
Particles density, ρ_s(kg/m^3)		2500
Small particles	d_p(mm)	0.4-0.6
	U_{mf}(m/s)	0.27
Medium particles	d_p(mm)	0.6-0.8
	U_{mf}(m/s)	0.44
Big particles	d_p(mm)	1-1.3
	U_{mf}(m/s)	0.67

A *Nikon* standard digital camera was used to record images of the front

wall of the fluidized bed at 60 fps. The spatial resolution of the pictures is 720 x 1280 pixels. The uncertainty in the discrimination of the solid phases is directly related to the spatial resolution of the image (i.e. the size of a pixel), which is $\sim$ 0.4 mm. A uniform illumination of the front of the bed was guaranteed with the use of two spotlights.

In each experiment, a partition was first inserted in the center of the bed to divide it into two equal parts (Figure 1). The left part was filled with black painted particles and the right part was filled with white particles. The bed aspect ratio was $H_0/W = 1$ in all the cases. After that, the partition was removed. Finally, the fluidizing air supply was turned on at the desired gas superficial velocity and the bed frontal view was recorded with the digital camera. The effect of the gas superficial velocity and the particle size on the solids mixing process in fluidized beds was analysed. To do that, three different particle sizes and gas velocities were tested, keeping constant the bed aspect ratio. A summary of the different experiments carried out is shown in Table 2.

Table 2: Summary of experiments.

Particle size (mm)	U_{mf} (m/s)	$U_0 - U_{mf}$ (m/s)		
1-1.3	0.67	0.67	1.005	1.34
0.6-0.8	0.44	0.44	0.66	0.88
0.4-0.6	0.27	0.27	0.405	0.54

3. Theory

3.1. Mixing index

The completely unmixed state is the state of maximum lateral segregation of the particles. In the particular case of a fluidized bed with non-reacting particles of two different colours (i.e. black and white), the maximum lateral segregation state is obtained when the white particles are located at one side of the bed and the black particles are located at the other side of the bed, as shown in Figure 3a.

The randomly mixed state is achieved when the particles are perfectly mixed and no preferential patterns can be observed. Random samples taken from a granular mixture in a randomly mixed state might contain a different

number of black particles each, however, from a global point of view the system is considered to be fully mixed. An example of the randomly mixed state in a fluidized bed with non-reacting particles of two colours can be seen in Figure 3b.

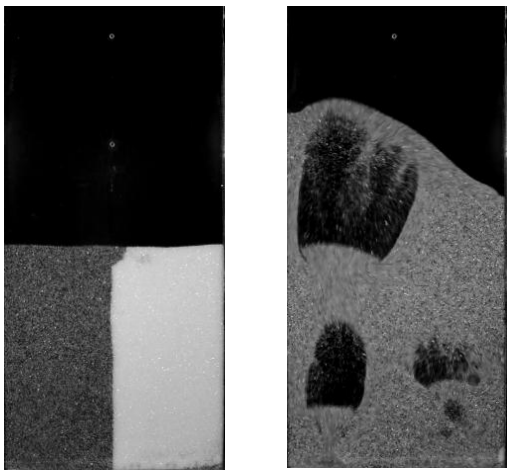

(a) (b)

Figure 3: Completely lateral segregated state (a) and randomly mixed state (b).

Therefore, the mixing process is defined as the process by which a system, starting in the completely segregated state, ends in the randomly mixed state. The quality of mixing can be assessed by examination of the degree of mixing of particles in the bed. The states of a granular mixture are condensed into probability distributions, which are further condensed into mixing indices by taking certain properties of that distributions. This process represents a cascade of information reduction, from the exact arrangement of particles in a mixture to the value of the mixing index [42].

Several mixing indices have been reported in the literature to describe the effectiveness of the mixing process, most of them were developed based on a statistical analysis of the mixing patterns. Some examples of mixing index are the entropy of mixing [43, 44], the Gini coefficient of mixing [45, 46] and the Lacey index [47]. The well-known Lacey index [47] is defined as:

$$M = \frac{S_0^2 - S^2}{S_0^2 - S_R^2} \tag{1}$$

where S_0^2 is the variance of the completely segregated state, S_R^2 is the variance of the randomly mixed state and S^2 is the variance of the mixture between the completely segregated state and the randomly mixed state. The Lacey index has a zero value for the completely segregated state and increases to unity for the randomly mixed state. Due to its simplicity, the Lacey index is widely used to characterize the mixing processes [6]. As reported by Lacey [47], the evolution of the mixing process with time follows an exponential trend towards the randomly mixed state.

3.2. Lateral dispersion coefficient

The mixing in the bed is assumed to be caused by bubbles rising and erupting at the bed surface. The fluidized bed dynamics is then a complex issue due to the interaction between bubbles and solids [2]. Bellgardt and Werther [33] reported that the vertical solids mixing is much faster than the lateral solids mixing. Taking it into account, the lateral solids mixing in a fluidized bed is commonly described as a random walk process, averaged by the 1D Fickian-type diffusion equation [3], which reads:

$$\frac{\partial C}{\partial t} = D_{sr} \frac{\partial^2 C}{\partial x^2} \tag{2}$$

where C is the concentration of tracer particles (i.e. black painted particles), D_{sr} is the lateral solids dispersion coefficient, t is the time and x is the spatial coordinate along the width of the bed. The lateral dispersion coefficient D_{sr} lumps the effects of various mechanisms responsible of solid mixing such as: wake transport, emulsion drifting, bubble coalescence and break-up [38]. To solve Equation 2, the initial and boundary conditions for the present case are:

$$\begin{cases} t = 0; 0 \leq x \leq W/2 & C{=}1 \quad (3a) \\ t = 0; W/2 \leq x \leq W & C{=}0 \quad (3b) \\ x = 0; x = W & \partial C/\partial x{=}0 \quad (3c) \end{cases}$$

The analytical solution of Equation 2 with the initial and boundary conditions is the following:

$$C = \frac{1}{2} + \frac{2}{\pi} \sum_{n=1}^{\infty} \frac{1}{n} \sin\left(\frac{n\pi}{2}\right) \cos\left(\frac{n\pi x}{W}\right) \exp\left(-\frac{n^2\pi^2}{W^2} D_{sr} t\right) \tag{4}$$

The values of C in Equation 4 ranges between 0 and 0.5 for x varying between 0 and $W/2$, and ranges between 1 and 0.5 for x between $W/2$ and W. To account for values of tracer concentration between 0 and 1, the concentration C was normalized with the initial tracer concentration, C_0, defined as the mass of tracer particles at the initial state divided by the total mass of particles in the bed. The normalized theoretical tracer concentration, C_t^*, with values between 0 and 1, is shown in Equation 5.

$$C_t^* = \frac{C}{C_0} = 1 + \frac{4}{\pi} \sum_{n=1}^{\infty} \frac{1}{n} \sin\left(\frac{n\pi}{2}\right) \cos\left(\frac{n\pi x}{W}\right) \exp\left(-\frac{n^2\pi^2}{W^2} D_{sr} t\right) \quad (5)$$

The values reported in the literature for D_{sr} in fluidized beds differ by several orders of magnitude. The studies carried out in large beds and at high fluidizing velocities report values of D_{sr} around 10^{-1} m^2/s, meanwhile the studies conducted in small scale fluidized beds report values of D_{sr} around 10^{-3} m^2/s [2]. A comparison of values of D_{sr} reported by several authors can be found in Olsson *et al.* [48].

4. Results and discussion

4.1. Image processing

For each experiment, every image was processed to recognize the level of white particles. Two different approaches were employed for the solid phase recognition. The first one consists on estimating how much solid phase can be considered fully mixed in each picture. Using this procedure, the initial state of the bed has an area of white region equal to half of the total white area (i.e. half of the bed frontal area). As long as the bed starts to mix, the black particles will move towards the white region, creating a new grey region that can be recognized as white region if the proper threshold is applied to the images [49]. The final state is reached when all the solid phase can be recognized as a white region. The second approach consist on estimating the rate of disappearance of the white area. In this procedure, the initial state has the theoretical maximum white area and the final state is reached when no white area is detected in the images. The grey region is recognized in this case as black region in the binarized image. Both procedures were compared and the second one showed better results, since the first algorithm was influenced by the fact that bubbles cannot be distinguished from the

black particles in these experiments. Therefore, the subsequent calculations are based on the white level disappearance procedure in the images processed.

Figure 4a shows several selected snapshots of a mixing experiment. The images correspond to the case of $(U_0 - U_{mf}) = 0.66$ m/s and $d_p = 0.6 - 0.8$ mm, the nominal case hereafter. In the first image (t = 0 s) the bed is in the completely lateral segregated state, then the black and white particles start to mix because of the effect of the rising bubbles and, finally, the bed reaches the randomly mixed state (t = 8.5 s).

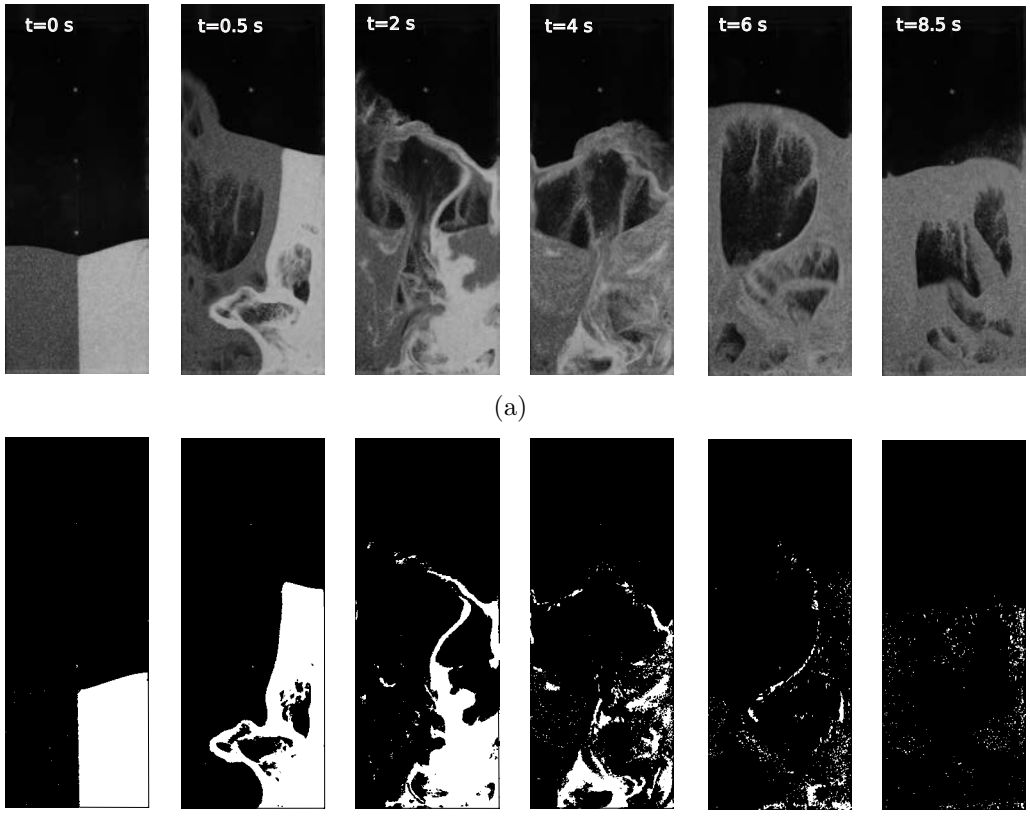

(a)

(b)

Figure 4: Example of a mixing process (a) and its image processing (b) ($(U_0 - U_{mf}) = 0.66$ m/s, $d_p = 0.6 - 0.8$ mm).

The Lacey index is usually applied to images previously divided into discrete cells and it could be only applied to the experiments of this work if

it were possible to distinguish between all phases present in the bed simultaneously (i.e. black solid phase, white solid phase and bubble phase). As long as the bed rear wall is also black, the black solid phase and the bubble phase cannot be differentiated in the images. Therefore, a modified mixing index is defined in Equation 6, based on Lacey index.

$$MI = 1 - \frac{A_{w,i}}{A_{w,max}} \tag{6}$$

where $A_{w,i}$ is the area of the white region of the image i and $A_{w,max}$ is the maximum area of the white region of all the images, which corresponds to a state where the bed has reached the maximum bed expansion. The white region of an image is defined as the region recognized as white once the image is binarized (Figure 4b). The mixing index, MI, defined in Equation 6 accounts for the variation of the concentration of white region in each image. Since black solid phase is usually treated as the tracer phase, the normalized tracer concentration, C^*, is defined in Equation 7.

$$C^* = 1 - MI \tag{7}$$

4.2. Mixing index

The normalized mixing index as a function of time, for the nominal case, is shown in Figure 5.

As can be observed, the mixing curve can be divided in different sections. The first one is the start-up section, where transient effects of the sudden air input are noticeable. Here, the mixing index decreases due to the initial bed expansion produced when the air is injected. The start-up section ends when the bed reaches the state of maximum bed expansion. This is followed by a mixing section, where the mixing index increases with time following an exponential trend. The last section corresponds to the randomly mixed state, where the bed can be considered fully mixed and the solids mixing process has reached the steady state. Considering the different mixing mechanisms reported in the literature [47], the mixing region can be divided into two sections. The first section shows a fast increase of the mixing index, which seems to be dominated by convective mixing, mainly governed by bubbles capable of transporting a high amount of particles. After that fast increase of the mixing index, the mixing speed is reduced before it reaches the randomly mixed state. Here, bubbles can no longer break the small clusters of

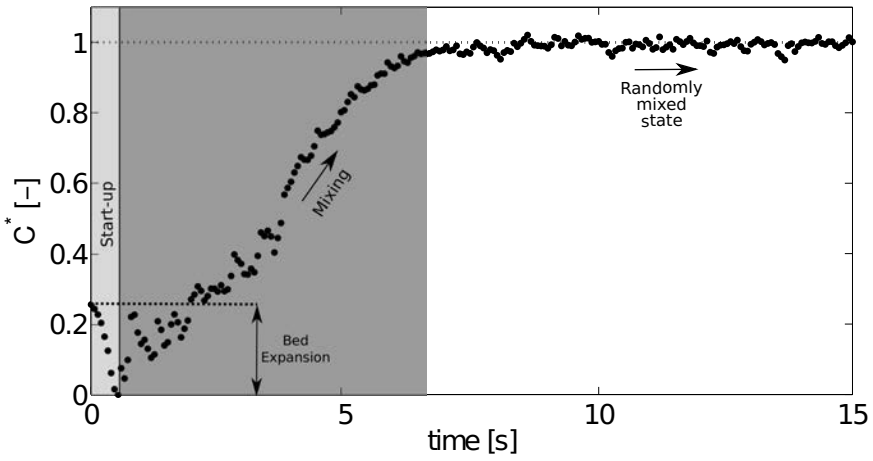

Figure 5: Mixing index as a function of time ($(U_0 - U_{mf}) = 0.66$ m/s, $d_p = 0.6 - 0.8$ mm).

particles of the same colour and, therefore, this mixing region is dominated by diffusion.

The time evolution of the mixing index was obtained for the three particle sizes and the three superficial gas velocities summarized in Table 2. The results are shown in Figure 6. As can be observed, the time to reach the randomly mixed state decreases when the gas velocity is increased, for the three particle sizes investigated. A higher velocity generates more bubbles, increasing the solids movement inside the bed and enhancing the mixing process. For the case of $d_p = 1 - 1.3$ mm (Figure 6c), both the experiments at $U_0 - U_{mf} = 1.005$ m/s and at $U_0 - U_{mf} = 1.34$ m/s reach the randomly mixed state almost at the same time. These experiments correspond to the highest excess gas velocities, $U_0 - U_{mf}$, tested and the bubble size might be high enough to consider that the bed have reached a maximum mixing velocity, and consequently a minimum mixing time. Beyond that point, a higher velocity would not decrease the mixing time, independently of the particle size, for the range of particle sizes tested in this work.

To evaluate the effect of the gas velocity and particle size on the mixing time, t_{95} is defined as the time at which the mixing index of Equation 6 reaches a value of 0.95. The results of t_{95} are plotted in Figure 7 as a function of the excess gas velocity, $U_0 - U_{mf}$, for the three particle sizes investigated.

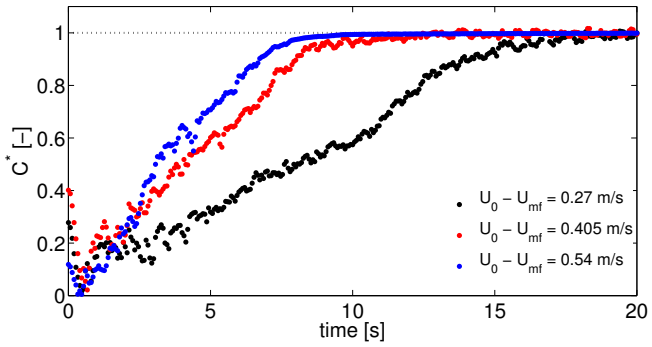

(a)

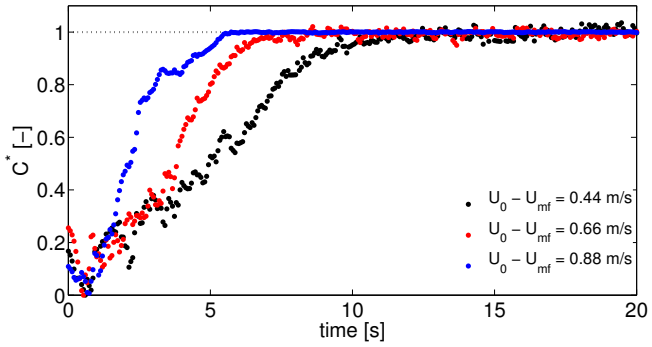

(b)

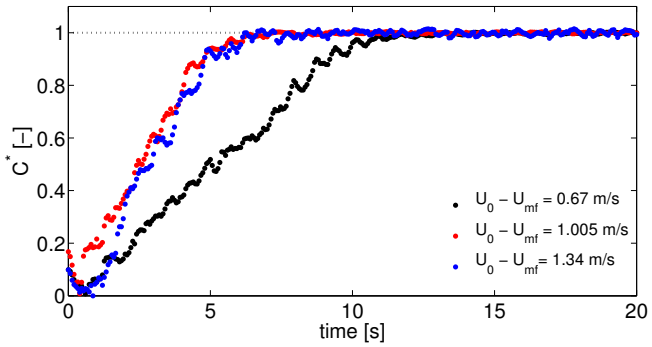

(c)

Figure 6: Mixing curves for the three excess gas velocities tested for $d_p = 0.4 - 0.6$ mm (a) $d_p = 0.6 - 0.8$ mm (b) and $d_p = 1 - 1.3$ mm (c).

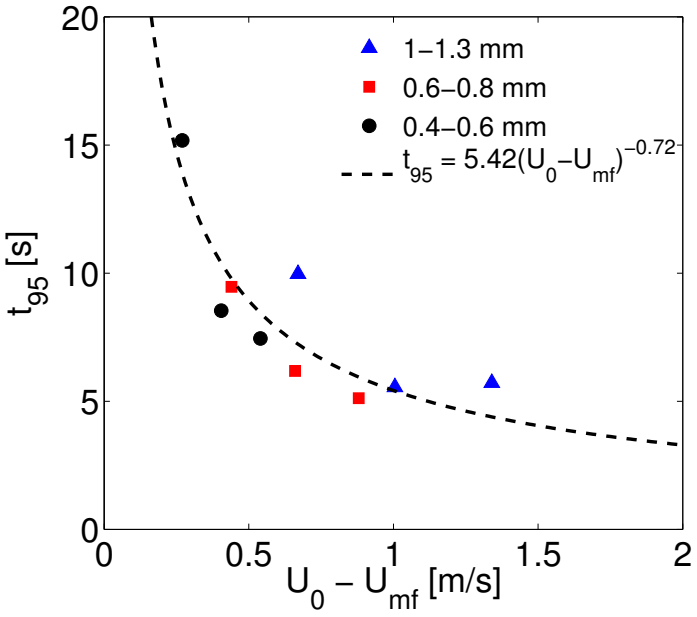

Figure 7: Mixing time, t_{95}, as a function of the excess gas velocity, $U_0 - U_{mf}$, for the three particle sizes investigated.

As stated above, the value of t_{95} decreases with the excess gas velocity. A potential fitting of the experimental data of t_{95} as a function of the excess gas velocity was proposed. As can be observed in Figure 7, the potential fitting seems to predict quite well the variation of t_{95} with the excess gas velocity, suggesting that the effect of the particle size has a small importance compared to the effect of the gas velocity.

The start-up time, t_{start}, was also characterized. The values of t_{start} were found to be barely constant around 0.5 s for all the cases investigated, therefore it is not influenced by the excess gas velocity nor the particle size. The start-up section seems to be affected by the way the experiment is carried out, which means that can be characterized and compared only for experiments carried out under the same experimental conditions. Therefore, as long as this zone is strongly influenced by the way the experiments are carried out, it has to be eliminated to perform accurate fittings of the diffusive mixing section to the solution of the diffusion equation (Equation 5).

As stated before, the solids mixing mechanism in fluidized beds is related to bubbles [6]. Since t_{95} accounts for the extent of the mixing process, the experimental values of t_{95} were compared with the values of the residence time of the bubbles in the bed, $t_{res,b}$, defined in Equation 8.

$$t_{res,b} = \int_0^{H_0} \frac{1}{U_b} dH \tag{8}$$

where U_b is the rising velocity of the bubbles. The bubble velocity was estimated with Equation 9, an expression reported by Shen *et al.* [8], based on the equation previously reported by Davidson and Harrison [50], to calculate the bubble velocity in pseudo-2D fluidized beds.

$$U_b = (U_0 - U_{mf}) + \phi \left(g d_b\right)^{1/2} \tag{9}$$

where d_b is the bubble diameter, g is the gravity and ϕ is the bubble velocity coefficient, which is equal to 1 in this case. The correlation of Shen *et al.* [8] was used to estimate the values of d_b, as can be seen in Equation 10.

$$d_b = 0.89 \left[(U_0 - U_{mf}) \left(H + 3 \left(A_0/Z\right)\right)\right]^{2/3} g^{-1/3} \tag{10}$$

where A_0 is the area of the distributor per orifice and Z the bed thickness. The correlation of Shen *et al.* [8] has been previously proven to give good estimations of both bubble diameter and velocity in pseudo-2D fluidized beds [10, 12–15]. In Figure 8, the experimental values of t_{95} are plotted as a function of the estimated values of the residence time of the bubbles in the bed, $t_{res,b}$.

As can be observed, the experimental data of t_{95} follows a linear trend with $t_{res,b}$. The residence time of bubbles in the bed, $t_{res,b}$, accounts for the vertical movement of bubbles, related to the vertical solids mixing mechanism, and t_{95} accounts for the diffusive mixing, which is mainly related to the lateral solids mixing mechanism. Taking it into account, the linear fitting equation of Figure 8 represents the relation between vertical and lateral mixing. Therefore, the slope of the linear equation indicates that vertical mixing is almost 50 times faster than lateral mixing. This result is in accordance with previous studies [27, 51] and confirms that a 1D Fickian-type diffusion equation (Equation 2) can be used to fit the experimental data and to estimate the value of D_{sr}.

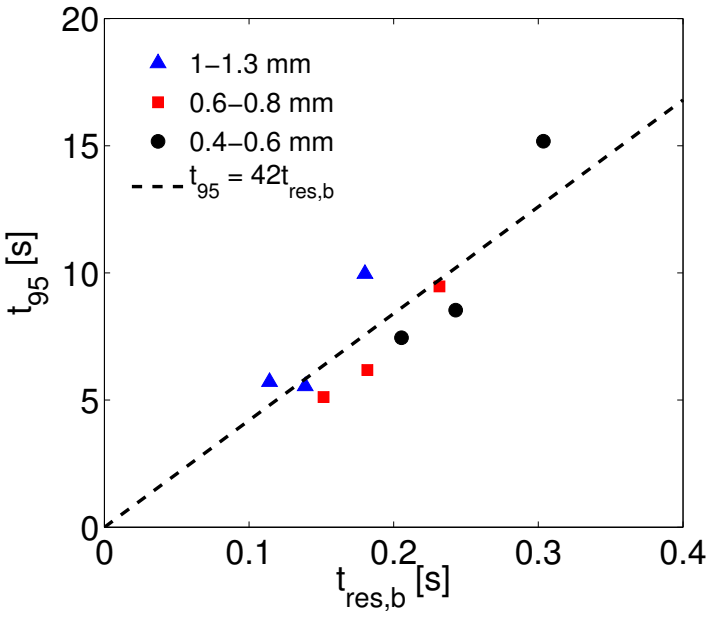

Figure 8: Mixing time, t_{95}, as a function of the residence time of the bubbles in the bed, $t_{res,b}$, for the three particle sizes investigated.

4.3. Lateral dispersion coefficient

According to the results of the previous section, to obtain D_{sr} a fitting of the experimental data of the normalized tracer concentration, C^*, to the solution of the diffusion equation (Equation 5) is proposed. Since the solution of the diffusion equation depends on the spatial coordinate, x, a spatial average from the origin of the coordinate system should be performed. Once the spatial average is performed, the value of D_{sr} that minimizes the error is selected. It is worth to notice that the absolute error, defined as the difference between C^* and C_t^*, was used as the criteria to select D_{sr} instead of using the quadratic error, because the quadratic error gives more significance to the errors in the part near the steady state. The values of D_{sr} obtained for the three gas superficial velocities and particle sizes investigated are plotted in Figure 9.

As can be observed, D_{sr} increases with the excess gas velocity. The experimental results of D_{sr} were compared to the predictions of the correlation

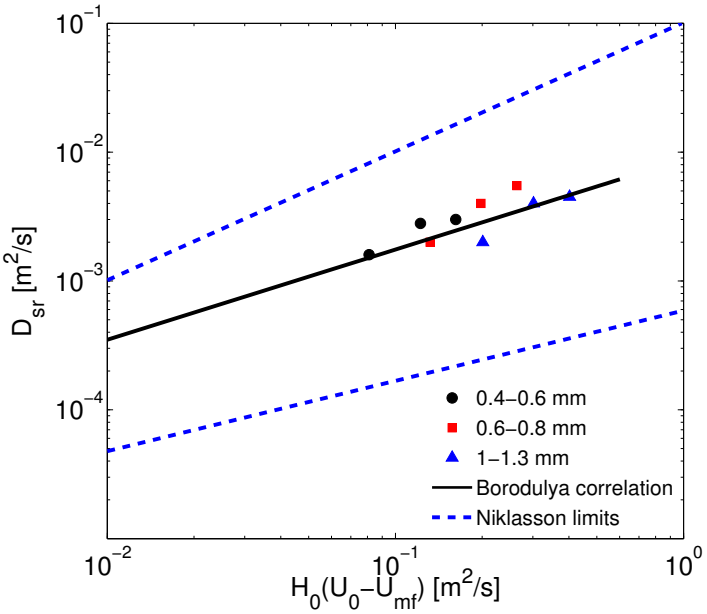

Figure 9: Experimental values of D_{sr} compared to the predictions of the correlation of Borodulya *et al.* [28] and the limits reported by Niklasson *et al.* [2].

of Borodulya *et al.* [28] (Equation 11).

$$D_{sr} = 0.013 H_0 \left(U_0 - U_{mf}\right) \left(\frac{D_C}{H_0}\right)^{0.5} Fr^{-0.15} \tag{11}$$

where D_C is the equivalent bed diameter ($D_C = \sqrt{4WZ/\pi}$) and Fr is the Froude number ($Fr = (U_0 - U_{mf})^2/gH_0$). This correlation was developed based on thermal diffusivity experiments, thus the authors actually measured the thermal diffusivity. Salam *et al.* [52] reported that the thermal diffusivity is only 55% of the lateral dispersion coefficient in a fluidized bed. According to that, the values of D_{sr} obtained with Borodulya *et al.* [28] correlation were corrected and plotted in Figure 9 for the range of experimental values of $H_0(U_0 - U_{mf})$ reported by the authors. The corrected correlation of Borodulya *et al.* [28] seems to predict quite well the trend of the experimental values of D_{sr}, indicating that D_{sr} is independent of the particle size, which is in agreement with the previous results of the present work. The range of

experimental values of D_{sr} reported in the literature by Niklasson *et al.* [2] was also plotted in Figure 9 to show that the experimental values of D_{sr} of the the present work lie within this range.

4.4. Relation between the mixing time and the lateral dispersion coefficient

Once the mixing index, related to t_{95}, and the lateral dispersion coefficient, D_{sr}, were studied separately, the relation between both parameters was investigated. In Figure 10, the experimental values of D_{sr} shown in Figure 9 were compared to the experimental values of t_{95} shown in Figure 7. The lateral dispersion coefficient, D_{sr}, is inversely proportional to t_{95}. As can be seen in Figure 10 there is a potential relation between D_{sr} and t_{95}.

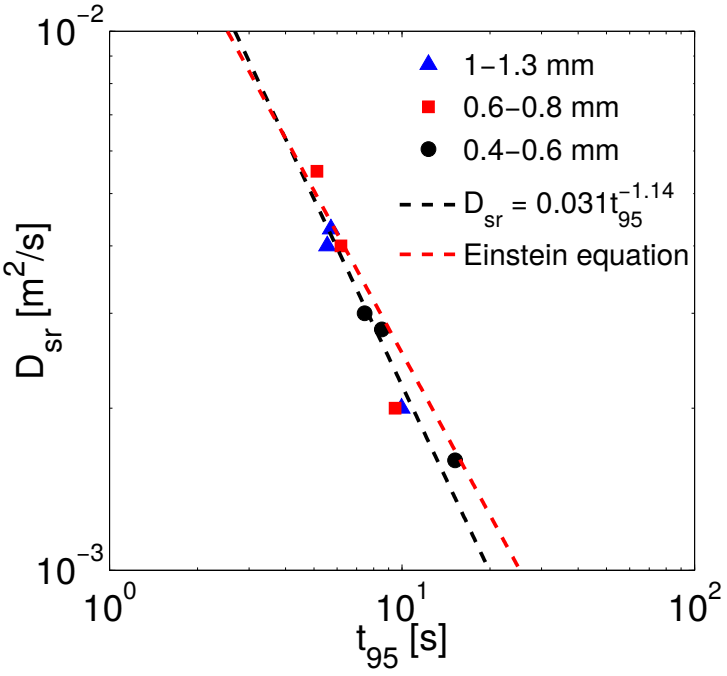

Figure 10: Experimental values of D_{sr} as a function of the experimental values of t_{95}.

This result means that both D_{sr} and t_{95} are directly related and this relation can be expressed by Equation 12:

$$D_{sr} = 0.031 t_{95}^{-1.14} \tag{12}$$

By means of Equation 12, the value of t_{95} can be estimated using D_{sr}, and vice versa. The value of D_{sr} may be obtained either with correlations (i.e. Borodulya *et al.* [28]) or experimentally, independently of the experimental method used, and with this value, the solids mixing time, t_{95}, can be determined.

Equation 13 shows the Einstein's equation [53], which provide a relation of the dispersion coefficient with the average displacement and the time elapsed in that displacement, according to the theory of the brownian movement.

$$D_{sr} = \frac{\Delta x^2}{2\tau} \tag{13}$$

where Δx is the average displacement of a tracer particle and τ is the dispersive mixing time. The value of Δx for the experimental conditions of the present work was determined dividing the initial black solid phase into n regions and averaging the displacement of an individual tracer particle from each of that regions to the opposite edge of the bed. The value of Δx was determined to be $(3/4)W$.

The estimated values of D_{sr} of the Einstein's equation were also plotted in Figure 10. As can be observed in Figure 10, the estimations of the Einstein's equation are in good agreement with the experimental results of D_{sr} obtained in the present work.

The results presented regarding the characteristic mixing time are restricted to the operational conditions tested and the geometry of the bed. Nevertheless, the connection with the lateral dispersion coefficient could be generalized as it shows a quite good agreement with the Borodulya *et al.* [28] correlation in spite of a practical validation with further operational conditions and bed geometries. Concerning the extrapolation of the results of this work to very different geometries and solid particle sizes, the estimations obtained should be validated.

5. Conclusions

A new methodology has been proposed to estimate the lateral dispersion coefficient by means of an experimental visualization technique. The methodology can be used to estimate both the mixing time and the lateral dispersion coefficient.

Regarding the mixing index study, two different zones were found in the mixing experiments. The first zone corresponds to the start-up process and

the second zone corresponds to the mixing process. The start-up time was characterized and it was observed that it remains barely constant around 0.5 s. The total mixing time, t_{95}, was also characterized and it was found that it is influenced by the excess gas velocity, but the effect of the particle size on the mixing time is negligible, in accordance to previously reported works in the literature. The experimental results of t_{95} were compared to the estimated values of the residence time of the bubbles in the bed, $t_{res,b}$, and it can be concluded that the vertical solids mixing is around 50 times faster than the lateral solids mixing, justifying the use of the 1D Fickian-type diffusion equation to describe the mixing of solids in fluidized beds.

Regarding the lateral dispersion coefficient, the methodology was successfully applied to estimate the lateral dispersion coefficient from experimental visualization data. It has been proven that it is not necessary to distinguish between the bubbles and the tracers (i.e. black painted particles) to apply a visualization method in the estimation of the lateral dispersion coefficient. The experimental data of the normalized tracer concentration was averaged along the spatial coordinate and fitted to the solution of the 1D diffusion equation. The correlation of Borodulya *et al.* [28] was found to predict quite well the experimental values of the lateral dispersion coefficient, which is in accordance with the previous results of this work regarding the negligible effect of the particle size on the lateral dispersion coefficient.

Finally, the experimental values of t_{95} and D_{sr} obtained in the present work were linked. It was concluded that both parameters are inversely proportional and they are related by a potential law. An expression was proposed to estimate t_{95} as a function of D_{sr} and vice versa. The experimental results of $D_s r$ also showed a good agreement with the predictions of the Einstein's equation of the theory of the brownian movement.

6. Notation

A_0	Area of the distributor per orifice (m^2)
$A_{w,max}$	Area of the white region of the expanded bed (px^2)
$A_{w,i}$	Area of the white region of the image i (px^2)
C	Tracer particles concentration (-)
C_0	Initial tracer particles concentration (-)
C^*	Normalized tracer particle concentration (-)
C_t^*	Normalized theoretical tracer particle concentration (-)
D_C	Equivalent diameter (m)

D_{sr}	Lateral dispersion coefficient (m^2/s)
d_b	Bubble diameter (m)
d_p	Mean particle diameter (mm)
Fr	Froude number (-)
g	Gravity (m/s^2)
H	Bed height (m)
H_0	Fixed bed height (m)
H_0/W	Bed aspect ratio (-)
M	Lacey mixing index (-)
MI	Modified mixing index (-)
ΔP_{dist}	Distributor pressure drop (kPa)
R	Distributor to bed pressure drop ratio (-)
S^2	Variance of the mixture under study (-)
S_0^2	Variance of the completely segregated state (-)
S_R^2	Variance of the randomly mixed state (-)
t	Time (s)
t_{95}	Time at which $MI = 0.95$ (s)
$t_{res,b}$	Residence time of the bubbles in the bed (s)
t_{start}	Start-up time (s)
U_0	Air superficial velocity (m/s)
U_b	Bubble velocity (m/s)
U_{mf}	Minimum fluidization velocity (m/s)
x	Spatial coordinate (m)
W	Bed width (m)
Z	Bed thickness (m)

Greek letters

Δx	Average displacement of a tracer particle (m)
ϕ	Bubble velocity coefficient (-)
ρ_s	Particle density (kg/m^3)
τ	Dispersive mixing time (s)

Abbreviattions

BFB	Bubbling fluidized bed.
DEM	Discrete element model.

DIA	Digital image analysis.
FSS	Full-scale span.
RPT	Radioactive Particle Tracking.
SEM	Scanning Electron Microscope.

References

[1] D. Kunii, O. Levenspiel, *Fluidization engineering*, (1991) Butterworth-Heinemann, Stoneham, UK, 2nd ed.

[2] F. Niklasson, H. Thunman, F. Johnsson, B. Leckner, Estimation of solids mixing in a fluidized-bed combustor, *Ind. Eng. Chem. Res.* 41 (2002) 4663-4673.

[3] D. Liu and X. Chen, Lateral solids dispersion coefficient in large-scale fluidized beds, *Combust. Flame* 157 (2010) 2116-2124.

[4] L.M. Garcia-Gutierrez, A. Soria-Verdugo, U. Ruiz-Rivas, Optimization of the feeding ports location in a fluidized bed combustor based on Monte Carlo simulations of fuel particles motion, *Fuel* 141 (2015) 82-92.

[5] G.A. Bokkers, M. van Sint Annaland, J.A.M. Kuipers, Mixing and segregation in a bidisperse gas-solid fluidized bed: a numerical and experimental study, *Powder Technol.* 140 (2004) 176-186.

[6] M.J. Rhodes, X.S. Wang, M. Nguyen, P. Stewart, K. Liffman, Study of mixing in gas-fluidized beds using a DEM model, *Chem. Eng. Sci.* 56 (2001) 2859-2866.

[7] I. Eames, M.A. Gilbertson, Mixing and drift in gas-fluidised beds, *Powder Technol.* 154 (2005) 185-193.

[8] L. Shen, F. Johnsson, B. Leckner, Digital image analysis of hydrodynamics two-dimensional bubbling fluidized beds, *Chem. Eng. Sci.* 59 (2004) 2607-2617.

[9] C.R. Müller, J.F. Davidson, J.S. Dennis, A.N. Hayhurst, A study of the motion and eruption of a bubble at the surface of a two-dimensional fluidized bed using particle image velocimetry (PIV), *Ind. Eng. Chem. Res.* 46 (2007) 1642-1652.

[10] J.A. Laverman, I. Roghair, M. van Sint Annaland, J.A.M. Kuipers, Investigation into the hydrodynamics of gas-solid fluidized beds using particle image velocimetry coupled with digital image analysis, *Can. J. Chem. Eng.* 86 (2008) 523-535.

[11] A. Busciglio, G. Vella, G. Micale, L. Rizzuti, Analysis of the bubbling behaviour of 2D gas solid fluidized beds: Part I. Digital image analysis technique, *Chem. Eng. J.* 140 (2008) 398-413.

[12] S. Sánchez-Delgado, C. Marugán-Cruz, A. Soria-Verdugo, D. Santana, Estimation and experimental validation of the circulation time in a 2D gas-solid fluidized bed, *Powder Technol.* 150 (2013) 1-8.

[13] A. Soria-Verdugo, L.M. Garcia-Gutierrez, S. Sánchez-Delgado, U. Ruiz-Rivas, Circulation of an object inmersed in a bubbling fluidized bed, *Chem. Eng. Sci.* 66 (2011) 78-87.

[14] A. Soria-Verdugo, L.M. Garcia-Gutierrez, N. García-Hernando, U. Ruiz-Rivas, Bouyancy effects on objects moving in a fluidized bed, *Chem. Eng. Sci.* 66 (2011) 2833-2841.

[15] F. Hernández-Jiménez, S. Sánchez-Delgado, A. Gómez-García, A. Acosta-Iborra, Comparison between two-fluid model simulations and particle image analysis & velocimetry (PIV) results for a two-dimensional gas-solid fluidized bed, *Chem. Eng. Sci.* 66 (2011) 3753-3772.

[16] F. Hernández-Jiménez, J.R. Third, A. Acosta-Iborra, C.R. Müller, Comparison of bubble eruption models with two-fluid simulations in a 2D gas-fluidized bed, *Chem. Eng. J.* 171 (2011) 328-339.

[17] F. Hernández-Jiménez, J. Sánchez-Prieto, A. Soria-Verdugo, A. Acosta-Iborra, Experimental quantification of particle-wall frictional forces in pseudo-2D gas fluidised beds, *Chem. Eng. Sci.* 102 (2013) 257-267.

[18] A.S. Hull, Z. Chen, P.K. Agarwal, Influence of horizontal tube banks on the behavior of bubbling fluidized beds: 2. Mixing of solids, *Powder Technol.* 111 (2000) 192-199.

[19] Y. Zhang, B. Jin, W. Zhong, Experiment on particle mixing in flat-bottom spout-fluid bed, *Chem. Eng. Process.* 48 (2009) 126-134.

[20] S. Gorji-Kandi, S.M. Alavi-Amleshi, N. Mostoufi, A solids mixing rate correlation for small scale fluidized beds, *Particuology* 21 (2015) 55-64.

[21] I. Julián, J. Herguido, M. Menéndez, Particle mixing in a two-section two-zone fluidized bed reactor. experimental technique and countercurrent back-mixing model validation, *Ind. Eng. Chem. Res.* 52 (2013) 13587-13596.

[22] I. Julián, J. Herguido, M. Menéndez, Experimental and simulated solids mixing and bubbling behavior in a scaled two-section two-zone fluidized bed reactor, *Chem. Eng. Sci.* 143 (2016) 240-255.

[23] D. Liu, S. Xiao, X. Chen, C. Bu, Investigation of solid mixing mechanisms in a bubbling fluidized bed using a DEM-CFD approach, *Asia-Pac. J. Chem. Eng.* 7(2) (2012) S237-S244.

[24] M. Fang, K. Luo, S. Yang, K. Zhang, J. Fan, Computational fluid dynamics discrete element method investigation of solid mixing characteristics in an internally circulating fluidized bed, *Ind. Eng. Chem. Res.* 52 (2013) 7556-7568.

[25] S. Yang, K. Luo, M. Fang, J. Fan, Influence of tube configuration on the gas-solid hydrodynamics of an internally circulating fluidized bed: a discrete element study, *Chem. Eng. J.* 239 (2014) 158-170.

[26] K. Luo, F. Wu, S. Yang, J. Fan, CFD-DEM study of mixing and dispersion behaviors of solid phase in a bubbling fluidized bed, *Powder Technol.* 274 (2015) 482-493.

[27] D. Bellgardt, M. Schoessler, J. Werther, Lateral non-uniformities of solids and gas concentrations in fluidized bed reactors, *AIChE Annual Meeting* 1986.

[28] V.A. Borodulya, Y.G. Epanov, Y.S. Teplitskii, Horizontal particle mixing in a free fluidized bed, *J. Eng. Phys. Thermophys.* 42 (1982) 528-533.

[29] L. Glicksman, E. Carr, P. Noymer, Particle injection and mixing experiments in a one-quarter scale model bubbling fluidized bed, *Powder Technol.* 180 (2008) 284-288.

[30] L. Shen and M. Zhang, Effect of particle size on solids mixing in bubbling fluidized beds, *Powder Technol.* 97 (1998) 170-177.

[31] Y.F. Shi, L.T. Fan, Lateral mixing of solids in batch gas-solids fluidized beds, *Ind. Eng. Chem. Process Des. Dev.* 23 (1982) 337-341.

[32] E. Sette, D. Pallarès, F. Johnsson, Experimental evaluation of lateral mixing of bulk solids in a fluid-dinamically down-scaled bubbling fluidized bed, *Powder Technol.* 263 (2014a) 74-80.

[33] D. Bellgardt and J. Werther, A novel method for the investigation of particle mixing in gas-solid systems, *Powder Technol.* 48 (1986) 173-180.

[34] N. Mostoufi and J. Chaouki, On the axial movement of solids in gas-solid fluidized beds, *Trans IChemE* 78 (2000) 911-920.

[35] E. Sette, D. Pallarès, F. Johnsson, Experimental quantification of lateral mixing of fuels in fluid-dynamically down-scaled bubbling fluidized beds, *Appl. Energy* 136 (2014b) 671-681.

[36] E. Sette, T. Berdugo Vilches, D. Pallarès, F. Johnsson, Measuring fuel mixing under industrial fluidized-bed conditions - A camera-probe based fuel tracking system, *App. Energy* 163 (2016) 304-312.

[37] M. Farzaneh, S. Sasic, A.E. Almstedt, F. Johnsson, D. Pallarès, A study of fuel particle movement in fluidized beds, *Ind. Eng. Chem. Res.* 52 (2013) 5791-5805.

[38] O. Oke, P. Lettieri, P. Salatino, R. Solimene, L. Mazzei, Numerical simulations of lateral solid mixing in gas-fluidized beds, *Chem. Eng. Sci.* 120 (2014) 117-129.

[39] F.Hernández-Jiménez, L.M. García-Gutiérrez, A. Soria-Verdugo, A. Acosta-Iborra, Fully coupled TFM-DEM simulations to study the motion of fuel particles in a fluidized bed, *Chem. Eng. Sci.* 134 (2015) 57-66.

[40] S.B.R. Karri, J. Werther, Gas distributor and plenum design in fluidized beds. In: W.C. Yang, *Handbook of fluidization and fluid-particle systems.* Marcel Dekker Inc., New York, (2003) 164-179.

[41] J. Sánchez-Prieto, A. Soria-Verdugo, J.V. Briongos, D. Santana, The effect of temperature on the distributor design in bubbling fluidized beds, *Powder Technol.* 261 (2014) 176-184.

[42] Z. Gu, J.J.J. Chen, A probabilistic analysis of some selected mixing indices, *Chem. Eng. Res. Des.* 93 (2015) 293-303.

[43] K. Ogawa, S. Ito, A definition of quality of mixedness, *J. Chem. Eng. Jpn.* 8 (1973) 148-151.

[44] A. Guida, A.W. Nienow, M. Barigou, Shannon entropy for local and global description of mixing by Lagrangian particle tracking, *Chem. Eng. Sci.* 65 (2010) 2865-2883.

[45] A. Sen, On Economic Inequality. Clarendon Press, Oxford, pp.24-46.

[46] F. Trivellato, On the efficiency of turbulent mixing in rotating stirrers, *Chem. Eng. Process.: Process Intensif.* 45 (2011) 500-506.

[47] P.M.C. Lacey, Developments in the theory of particle mixing, *J. Appl. Chem.* 4 (1954) 257-268.

[48] J. Olsson, D. Pallares, F. Johnsson, Lateral fuel dispersion in a large-scale bubbling fluidized bed, *Chem. Eng. Sci.* 74 (2012) 148-159.

[49] Otsu, N., A threshold selection method from gray-level histograms, *IEEE Transactions on Systems Man and Cybernetic*s 9 (1979) 62-66.

[50] J.F. Davidson and D. Harrison, *Fluidized particles*, (1963) Cambridge Univ. Press, New York.

[51] N. Mostoufi, J. Chaouki, Local solid mixing in gassolid fluidized beds, *Powder Technol.* 114 (2001) 23-31.

[52] T.F. Salam, Y. Ren, B.M. Gibbs, Lateral solid and thermal dispersion in fluidized bed combustors, *Proc. Int. Conf. Fluid Bed Combust.* 9 (1987) 541.

[53] A. Einstein, *Investigations on the theory of the brownian movement*, (1956) Dover Publications Inc.